

# A family of triaxial modified Hubble mass models: effects of the additional radial functions

Mousumi Das<sup>a</sup>, Parijat Thakur<sup>a,\*</sup>, H.B. Ann<sup>a</sup>,

<sup>a</sup>*Division of Science Education, Pusan National University, Busan 609-735, Korea*

---

## Abstract

The projected properties of triaxial generalization of the modified Hubble mass models are studied. These models are constructed by adding the additional radial functions, each multiplied by a low-order spherical harmonic, to the models of Chakraborty & Thakur (2000). The projected surface density of mass models can be calculated analytically which allows us to derive the analytic expressions of axial ratio and position angles of major axis of constant density elliptical contours at asymptotic radii. The models are more general than those studied earlier in the sense that the inclusions of additional terms in density distribution, allows one to produce varieties of the radial profile of axial ratio and position angle, in particular, their small scale variations at inner radii. Strong correlations are found to exist between the observed axial ratio evaluated at  $0.25R_e$  and at  $4R_e$  which occupy well-separated regions in the parameter space for different choices of the intrinsic axial ratios. These correlations can be exploited to predict the intrinsic shape of the mass model, independent of the viewing angles. Using Bayesian statistics, the result of a test case launched for an estimation of the shape of a model galaxy is found to be satisfactory.

*Key words:* galaxies : triaxial - galaxies : photometry - galaxies : structure.

---

## 1 Introduction

Observed photometric properties of majority of elliptical galaxies show isophotal twists and variations in ellipticity and position angle of major axis with

---

\* Corresponding author.

*Email addresses:* [mdas@pusan.ac.kr](mailto:mdas@pusan.ac.kr) (Mousumi Das), [pthakur@pusan.ac.kr](mailto:pthakur@pusan.ac.kr) (Parijat Thakur), [hbann@pusan.ac.kr](mailto:hbann@pusan.ac.kr) (H.B. Ann).

radius. These observed properties can be produced in a natural way by triaxial models. Chakraborty & Thakur (2000, hereafter CT00) studied the projected properties of a family of mass models which are triaxial generalisation of modified Hubble mass model. The model was first proposed by Schwarzschild (1979) as a numerical model for a triaxial stellar system in dynamical equilibrium and later casted into analytical form by de Zeeuw & Merritt (1983). It was found by CT00 that these models show ellipticity variations and isophotal twists in their projections along the line of sight. Moreover, the radial profiles of the parameters of the elliptical isophotes were found to be smooth functions of the radius (see CT00). However, many elliptical galaxies, devoid of any features, indicating the absence of shells or dust, are found to exhibit small scale variations in the radial profiles of the parameters of elliptical isophotes. This indicates that density distributions of such ellipticals may be more complex than that of CT00.

Above fact inspired us to modify the models of CT00 by adding the additional radial functions, each multiplied by a low-order spherical harmonic. The projected surface density  $\Sigma$  of resultant mass model can be calculated analytically. This makes possible to investigate some of the projected properties analytically. We calculated the profiles of surface density  $\Sigma$ , axial ratio  $b/a$  and position angle  $\Theta_*$  of the major axis as functions of radius. The analytical expression of the  $\Sigma$  is very useful for the calculations of  $b/a$  and  $\Theta_*$ . In the asymptotic regions analytical expressions can be derived, while in the intermediate regions simple numerical methods can be adopted for these calculations. The inclusions of additional terms in the density distribution, allows us to produce varieties of the radial profile of  $b/a$  and  $\Theta_*$  that can be compared with photometric data of real galaxies.

It was shown by de Zeeuw & Carollo (1996) that the observed ellipticities and the position angle, at small and at large radii can be used to derive the intrinsic axial ratios of the mass model, as a function of the viewing angles. Since the viewing angles of galaxies are largely unknown, it will be worth-while to get an estimate of the intrinsic axial ratios independent of the viewing angles. In this regard, Statler & Fry (1994, hereafter SF94), and Thakur & Chakraborty (2001, hereafter TC01) found that in case the observed parameters exhibit correlations when a model with a given set of intrinsic parameters is viewed in all possible orientations, one can obtain a probable estimate of the intrinsic shape, independent of the viewing angles. Furthermore, it was also shown by TC01 that the intrinsic shapes of triaxial mass models can be estimated using photometric properties and further, the results of shape estimation would be insensitive to the choice of models, if one considers ensembles of models which represent above mentioned correlations between the observed parameters. Thus, another aim of our present study is to build ensembles of models showing the correlations between observed parameters so that one could get an estimate of model independent shape.

In §2, we describe the mass model and in §3, we present the projected properties. Our results are described in §4, and §5 is devoted to summary and discussion.

## 2 The mass model

We modified the triaxial potential, given in de Zeeuw & Merritt (1983), corresponding to the density distribution considered in CT00 by adding the additional radial functions  $v_e(r)$  and  $w_e(r)$ , each multiplied by a low-order spherical harmonic. Thus, our assumed potential  $V(r, \theta, \phi)$  has a following form

$$V(r, \theta, \phi) = u(r) - (v(r) + v_e(r))Y_2^0(\theta) + (w(r) + w_e(r))Y_2^2(\theta, \phi), \quad (1)$$

where  $u(r)$ ,  $v(r)$ ,  $w(r)$ ,  $v_e(r)$  and  $w_e(r)$  are five radial functions,  $(r, \theta, \phi)$  are spherical coordinates defined such that  $x = r \sin \theta \cos \phi$ ,  $y = r \sin \theta \sin \phi$  and  $z = r \cos \theta$ , and  $Y_2^0(\theta) = \frac{3}{2}\cos^2\theta - \frac{1}{2}$  and  $Y_2^2(\theta, \phi) = 3\sin^2\theta\cos 2\phi$  are the usual spherical harmonics.

We take  $u(r)$  to be the potential of the spherical modified Hubble mass model, defined by

$$u(r) = -GM \frac{\ln[r + \sqrt{b_o^2 + r^2}]}{r}, \quad (2)$$

where  $M$  is the total mass of the model and  $b_o$  is the scale length. We choose  $v(r)$  and  $w(r)$  to be same as adopted in de Zeeuw & Merritt (1983) and reproduced below with slightly different notations.

$$\begin{aligned} v(r) &= -\frac{GM}{b_o^3} \frac{b_1^3 r^2}{(b_2^2 + r^2)^{3/2}} \\ w(r) &= -\frac{GM}{b_o^3} \frac{b_3^3 r^2}{(b_4^2 + r^2)^{3/2}}, \end{aligned} \quad (3)$$

where  $b_1, \dots, b_4$  are constants. The additional radial functions  $v_e(r)$  and  $w_e(r)$  are chosen such that they are effective in intermediate range of  $r$  only and not at small and at large radii. In order to satisfy this condition, a suitable choice of  $v_e(r)$  and  $w_e(r)$  are

$$v_e(r) = -\frac{GM}{b_o^3} \frac{a_1^4 r^6}{(a_2^2 + r^2)^4}$$

$$w_e(r) = -\frac{GM}{b_o^3} \frac{a_3^4 r^6}{(a_4^2 + r^2)^4}, \quad (4)$$

where  $a_1, \dots, a_4$  are constants. We note that  $v(r)$  and  $w(r)$  go as  $-r^2$  at small radii and as  $-1/r$ , at large radii. On the other hand,  $v_e(r)$  and  $w_e(r)$  go as  $-r^6$  at small radii and as  $-1/r^2$  at large radii.

For the above considered potential, the associated density distribution  $\rho(r, \theta, \phi)$  follows from Poisson's equation

$$\rho(r, \theta, \phi) = f(r) - (g(r) + g_e(r)) Y_2^0(\theta) + (h(r) + h_e(r)) Y_2^2(\theta, \phi). \quad (5)$$

The five radial functions appeared in equation (5) are given by

$$\begin{aligned} f(r) &= \frac{M}{4\pi} \frac{1}{(b_o^2 + r^2)^{3/2}}, \\ g(r) &= \frac{3M}{4\pi} \frac{b_1^3}{b_o^3} \frac{2r^4 + 7b_2^2 r^2}{(b_2^2 + r^2)^{7/2}}, \\ g_e(r) &= \frac{M}{4\pi} \frac{4a_1^4}{b_o^3} \frac{r^8 + 12a_2^2 r^6 - 9a_2^4 r^4}{(a_2^2 + r^2)^6}, \\ h(r) &= \frac{3M}{4\pi} \frac{b_3^3}{b_o^3} \frac{2r^4 + 7b_4^2 r^2}{(b_4^2 + r^2)^{7/2}}, \\ h_e(r) &= \frac{M}{4\pi} \frac{4a_3^4}{b_o^3} \frac{r^8 + 12a_4^2 r^6 - 9a_4^4 r^4}{(a_4^2 + r^2)^6}. \end{aligned} \quad (6)$$

The radial dependence of additional functions  $g_e(r)$  and  $h_e(r)$  in the density distribution are such that at asymptotic radii, the density remains same as that of CT00. At large radii,  $g_e(r)$  and  $h_e(r)$  decrease as  $r^{-4}$ , whereas  $g(r)$  and  $h(r)$  decrease as  $r^{-3}$ . Likewise, at small radii,  $g_e(r)$  and  $h_e(r)$  decrease as  $r^4$ , whereas  $g(r)$  and  $h(r)$  goes as  $r^2$ . Thus, the radial functions  $f(r)$ ,  $g(r)$  and  $h(r)$  are dominating at small and at large radii in the density distribution (5). The four ratios  $(b_1/b_o)$ ,  $\dots$ ,  $(b_4/b_o)$ , appeared in  $g(r)$  and  $h(r)$ , are expressed in terms of axial ratios of the approximately ellipsoidal constant  $\rho$  surfaces at small and at large radii by the same way as adopted in CT00. Prescribing the values of axial ratios of the approximately ellipsoidal constant  $\rho$  surfaces at very large and at very small radii as  $(p_\infty, q_\infty)$  and  $(p_o, q_o)$ , respectively, we find that

$$\begin{aligned} \left(\frac{b_1}{b_o}\right)^3 &= \frac{(1 + p_\infty^3 - 2q_\infty^3)}{6(1 + p_\infty^3 + q_\infty^3)}, \\ \left(\frac{b_3}{b_o}\right)^3 &= \frac{(1 - p_\infty^3)}{12(1 + p_\infty^3 + q_\infty^3)}, \end{aligned}$$

$$\begin{aligned}\left(\frac{b_2}{b_0}\right)^5 &= \left[ \frac{1 + p_\infty^3 - 2q_\infty^3}{6(1 + p_\infty^3 + q_\infty^3)} \right] \left[ \frac{7(p_0^2 + 4q_0^2 - 1)}{1 + p_0^2 - 2q_0^2} \right], \\ \left(\frac{b_4}{b_0}\right)^5 &= \left[ \frac{1 - p_\infty^3}{12(1 + p_\infty^3 + q_\infty^3)} \right] \left[ \frac{42(p_0^2 + 4q_0^2 - 1)}{2 - 6q_0^2} \right].\end{aligned}\quad (7)$$

Here it is clear that the expressions of  $(b_1/b_0)$  and  $(b_3/b_0)$  are exactly similar to those of CT00, whereas they are found to be completely different for  $(b_2/b_0)$  and  $(b_4/b_0)$ . Moreover, throughout the paper, the constant parameters  $a_1, \dots, a_4$  are chosen such that  $|g_e(r)| \ll |g(r)|$  and  $|h_e(r)| \ll |h(r)|$  at all  $r$ .

### 3 Projected properties

#### 3.1 Projected surface density

The density form (5) of the models allows a straight forward calculation of the projected surface density  $\Sigma$  for any viewing angle. We adopted the convention of de Zeeuw & Franx (1989) to project the model along line-of-sight. We chose coordinates  $(x', y', z')$  such that  $z'$ -axis runs along the line-of-sight, and  $x'$ -axis lies in the  $(x, y)$  plane. We considered  $(\theta', \phi')$  as the standard spherical coordinates of the line-of-sight and  $(R, \Theta)$  as the polar coordinates in  $(x', y')$  plane. The projected surface density  $\Sigma(R, \Theta)$  is obtained by integrating the model density along the line-of-sight,

$$\Sigma(R, \Theta) = \int_{-\infty}^{+\infty} \rho dz', \quad (8)$$

and after doing some intermediate calculations, it takes the following form

$$\Sigma(R, \Theta) = \Sigma_o(R) + \Sigma_2(R) \cos 2(\Theta - \Theta_*), \quad (9)$$

where

$$\begin{aligned}\Sigma_o(R) &= 2F_1 + \left(1 - 3 \cos^2 \theta'\right) \left[ (G_1 + G_{1e}) - \frac{3}{2}(G_2 + G_{2e}) \right] + \\ &\quad + [6(H_1 + H_{1e}) - 9(H_2 + H_{2e})] \sin^2 \theta' \cos 2\phi', \\ \Sigma_2^2(R) &= \left[ 6(H_2 + H_{2e}) \cos \theta' \sin 2\phi' \right]^2 + \left[ \frac{3}{2}(G_2 + G_{2e}) \sin^2 \theta' - \right. \\ &\quad \left. - 3(H_2 + H_{2e}) (1 + \cos^2 \theta') \cos 2\phi' \right]^2.\end{aligned}\quad (10)$$

We have defined the integrals

$$G_1(R) = \int_R^\infty \frac{r g(r) dr}{\sqrt{(r^2 - R^2)}}, \quad G_{1e}(R) = \int_R^\infty \frac{r g_e(r) dr}{\sqrt{(r^2 - R^2)}},$$

$$G_2(R) = R^2 \int_R^\infty \frac{g(r) dr}{r \sqrt{(r^2 - R^2)}}, \quad G_{2e}(R) = R^2 \int_R^\infty \frac{g_e(r) dr}{r \sqrt{(r^2 - R^2)}}, \quad (11)$$

and similarly integrals for  $F_1$ ,  $H_1$ ,  $H_2$ ,  $H_{1e}$  and  $H_{2e}$  in terms of functions  $f(r)$ ,  $h(r)$  and  $h_e(r)$ , respectively.

Above integrals are calculated analytically and can be expressed as

$$F_1(R) = \frac{M}{4\pi b_o^3} \frac{b_o^3}{b_o^2 + R^2},$$

$$G_1(R) = \frac{M}{4\pi b_o^3} \frac{2b_1^3}{(b_2^2 + R^2)^3} [2b_2^4 + 9b_2^2 R^2 + 3R^4],$$

$$G_{1e}(R) = \frac{M}{4\pi b_o^3} [4a_1^4 I_3 + 12a_2^2 I_2 - 9a_2^4 I_1],$$

$$G_2(R) = \frac{M}{4\pi b_o^3} \frac{4b_1^3}{(b_2^2 + R^2)^3} R^2 [3b_2^2 + R^2],$$

$$G_{2e}(R) = \frac{M}{4\pi b_o^3} [4a_1^4 R^2 I_2 + 12a_2^2 I_1 - 9a_2^4 I_4], \quad (12)$$

where

$$a_2^2 + R^2 = \alpha^2 \quad \beta = \frac{1}{512 \alpha^{11}},$$

$$I_1 = \beta(63R^4 + 14R^2\alpha^2 + 3\alpha^4),$$

$$I_2 = \beta(63R^6 + 21R^4\alpha^2 + 9R^2\alpha^4 + 3\alpha^6),$$

$$I_3 = \beta(63R^8 + 28R^6\alpha^2 + 18R^4\alpha^4 + 12R^2\alpha^6 + 7\alpha^8),$$

$$I_4 = \beta(63R^2 + 7\alpha^2). \quad (13)$$

Similarly,  $H_1(R)$  and  $H_2(R)$  can be written by substituting  $b_3$  and  $b_4$  in place of  $b_1$  and  $b_2$  in  $G_1(R)$  and  $G_2(R)$ , respectively. On the other hand,  $H_{1e}(R)$  and  $H_{2e}(R)$  are defined by substituting  $a_3$  and  $a_4$  in place of  $a_1$  and  $a_2$  in  $G_{1e}(R)$  and  $G_{2e}(R)$ , respectively.

The projected surface density (9) has its major axis at position angle  $\Theta_*$ , which is given by

$$\tan 2\Theta_* = \frac{T h_3}{h_1 + (1 - T) h_2}, \quad (14)$$

where  $h_1$ ,  $h_2$  and  $h_3$  depend only on the viewing angles  $(\theta', \phi')$  and are defined as

$$\begin{aligned} h_1 &= \sin^2 \phi' - \cos^2 \phi' \cos^2 \theta', \\ h_2 &= \cos^2 \phi' - \sin^2 \phi' \cos^2 \theta', \\ h_3 &= \sin 2\phi' \cos \theta'. \end{aligned} \quad (15)$$

The quantity  $T \equiv T(R)$  in equation (14) is the triaxiality parameter, which is given by

$$T \equiv T(R) = \frac{4 (H_2(R) + H_{2e}(R))}{(G_2(R) + G_{2e}(R)) + 2 (H_2(R) + H_{2e}(R))}. \quad (16)$$

Equation (14) gives the position angle  $\Theta_*$  of the major axis when it satisfies the condition

$$(H_2 + H_{2e})h_3 \sin 2\Theta_* < 0. \quad (17)$$

The observed axial ratio  $b/a$  of the projected surface density can be calculated by using the relation

$$\Sigma(b, \Theta_* - \frac{\pi}{2}) = \Sigma(a, \Theta_*), \quad (18)$$

which can be rewritten as

$$\Sigma_o(a) + \Sigma_2(a) = \Sigma_o(b) - \Sigma_2(b). \quad (19)$$

At a finite radial distance from the centre, the axial ratio can be calculated numerically using equation (19). However, at asymptotic limits, the analytical expressions can be obtained for  $b/a$ .

### 3.2 Projected properties at large and at small radii

The ratio  $(G_2 + G_{2e})/(H_2 + H_{2e})$  in (16) can be calculated analytically using (12), which in turn enables us to write an analytical expressions for  $T$  and  $\Theta_*$ . In particular, at large  $R$ , the ratio  $[(G_2 + G_{2e})/(H_2 + H_{2e})]_\infty$  and the triaxiality parameter  $T_\infty$  are given by

$$\left(\frac{G_2 + G_{2e}}{H_2 + H_{2e}}\right)_\infty = \frac{b_1^3}{b_3^3}, \quad (20)$$

and

$$T_\infty = \frac{4 b_3^3}{b_1^3 + 2 b_3^3} = \frac{1 - p_\infty^3}{1 - q_\infty^3}, \quad (21)$$

which clearly indicate that they are similar to  $(G_2/H_2)_\infty$  and triaxiality parameter at large  $R$  of CT00, respectively. Thus, the position angle  $\Theta_*$  at large  $R$  would also be identical to that of CT00 and can be calculated using equation (21) in (14).

Likewise, at small  $R$ , the ratio  $[(G_2 + G_{2e})/(H_2 + H_{2e})]_o$  and the triaxiality parameter  $T_o$  are

$$\left(\frac{G_2 + G_{2e}}{H_2 + H_{2e}}\right)_o = \frac{\frac{12b_1^3}{b_2^4} - \frac{33.13a_1}{a_2^{3/2}}}{\frac{12b_3^3}{b_4^4} - \frac{33.13a_3}{a_4^{3/2}}}, \quad (22)$$

and

$$T_o = \frac{4}{\left[2 + \frac{\frac{12b_1^3}{b_2^4} - \frac{33.13a_1}{a_2^{3/2}}}{\frac{12b_3^3}{b_4^4} - \frac{33.13a_3}{a_4^{3/2}}}\right]}. \quad (23)$$

It is clear that  $[(G_2 + G_{2e})/(H_2 + H_{2e})]_o$  and  $T_o$  differ much from  $(G_2/H_2)_o$  and triaxiality parameter at small  $R$  of CT00, respectively, which implies that the position angle  $\Theta_*$  at small  $R$  would also be much different than that of CT00.

We have used equation (19) to calculate the axial ratios at asymptotic radii. In order to write it in some particular form, we define a few more functions

$$\begin{aligned} h_4 &= (6 h_3)^2 + 9 (h_1 - h_2)^2, \\ h_5 &= \frac{9}{4} (h_1 + h_2)^2, \\ h_6 &= 9 (h_1^2 - h_2^2) \end{aligned} \quad (24)$$

of viewing angles  $(\theta', \phi')$  and then further define

$$Z \equiv \left[ h_4 + h_5 \left(\frac{G_2 + G_{2e}}{H_2 + H_{2e}}\right)^2 + h_6 \left(\frac{G_2 + G_{2e}}{H_2 + H_{2e}}\right) \right]^{1/2}, \quad (25)$$

and

$$\begin{aligned}
A &= \frac{\frac{12b_1^3}{b_2^4} - \frac{33.13a_1}{a_2^{3/2}}}{\frac{12b_3^3}{b_4^4} - \frac{33.13a_3}{a_4^{3/2}}}, \\
B &= \left\{ (4 \cos^2 \theta' \sin^2 2\phi')^2 + (3/2 \sin^2 2\phi')^2 A + (1 + \cos^2 \theta') \sin^2 \theta' \cos^2 2\phi' \right\}^{1/2}, \\
C &= -\frac{2}{b_o} + \frac{2b_1^3 h_4}{b_2^4} + \frac{72b_3^3 h_5}{b_4^4} + \frac{2a_1 A}{a_2^{3/2}} + \frac{12b_3^3}{b_4^4} B^{1/2}.
\end{aligned} \tag{26}$$

At very large  $R$ , the axial ratio is given by

$$\left(\frac{b}{a}\right)_\infty^2 = \frac{b_o^3 - 2b_3^3 Z_\infty}{b_o^3 + 2b_3^3 Z_\infty}, \tag{27}$$

where  $Z_\infty$  is the value of  $Z$  at very large  $R$  which can be evaluated by substituting the value of  $[(G_2 + G_{2e})/(H_2 + H_{2e})]_\infty$  from (20) in (25), i.e.,

$$Z_\infty \equiv \left[ h_4 + h_5 \left(\frac{b_1^3}{b_3^3}\right)^2 + h_6 \left(\frac{b_1^3}{b_3^3}\right) \right]^{1/2}. \tag{28}$$

On the other hand, at very small  $R$ , it can be expressed as

$$\left(\frac{b}{a}\right)_o^2 = \frac{C - 12B \frac{b_3^3}{b_4^4}}{C + 12B \frac{b_3^3}{b_4^4}}. \tag{29}$$

Thus, we find that the position angle  $\Theta_*$  of major axis and the axial ratio  $b/a$  are the same as those of CT00 at large radii, whereas they are much different at small radii. The reason behind this fact is that light from all radii will contribute to the projected properties evaluated at small radii and hence, the effects of additional radial functions are seen there.

## 4 Results

### 4.1 Radial profiles of the projected properties

The projected surface density  $\Sigma$  of our considered triaxial mass model (5) can be calculated analytically. Its approximate elliptical isodensity contours show the variations in the axial ratio  $b/a$  and the position angle  $\Theta_*$  of the major axis as functions of  $R$ . These features can be clearly seen from Fig. 1 where we present the radial profiles of  $\Sigma$ ,  $b/a$  and  $\Theta_*$  for particular choices of intrinsic axial ratios,  $p_o = p_\infty \equiv p$  and  $q_o = q_\infty \equiv q$ , the viewing angles  $(\theta', \phi')$  and the constant parameters  $(a_1, a_2, a_3, a_4)$ . On the basis of these results, our model can be considered as an example of simple analytical model showing ellipticity variations and isophotal twists in its projection along the line-of-sight. Since the resultant density distributing given in (5) can have different contributions of the additional radial functions  $g_e$  and  $h_e$  for the various choices of constant parameters  $(a_1, a_2, a_3, a_4)$ , in Fig. 2 we plotted the profiles of  $b/a$  as a function of  $R$  by allowing the different values of these constant parameters in such a manner that the resultant  $\rho$  must remain positive. In this way, the effects of additional radial functions on the profiles of  $b/a$  can be understood. We found that varieties of  $b/a$  profile can be produced by changing the constant parameters  $(a_1, a_2, a_3, a_4)$  whose trends are found to be different from each other. Besides, it has also been noticed that the inclusions of additional radial functions produce small scale variations in  $b/a$  profiles, specially at inner  $R$ , as compare to the smooth  $b/a$  profiles found in case of CT00. Moreover, the profiles of position angle  $\Theta_*$  also show small scale variation at inner  $R$  for different choices of the constant parameters  $(a_1, a_2, a_3, a_4)$  and in Fig. 3, we have shown it only for one case which has all the intrinsic parameters similar to those considered in bottom right panel of Fig. 2. The isodensity contours of many real elliptical galaxies show such small scale variations in the profiles of  $b/a$  and  $\Theta_*$  as functions of  $R$  rather than the smooth monotonically increasing or decreasing profiles of  $b/a$  and  $\Theta_*$  as those found in CT00. This suggests that the radial profiles of  $b/a$  and  $\Theta_*$  of our present triaxial models, as a function of viewing angles  $(\theta', \phi')$ , can be compared with observations.

### 4.2 Determination of observed projected properties exhibiting correlations

Determination of observed parameters which exhibit non-overlapping and well-separated correlations for different choices of intrinsic axial ratios is desirable problem since these parameters can be useful to get an estimate of intrinsic shapes of mass models, independent of viewing angles (SF94; TC01). It is also important to note here that correlation patterns between observed projected

properties evaluated at asymptotic radii, if exist, can save computing time due to availability of analytical expressions there. But, it would be meaningless to look for the correlations at asymptotic radii, since the observed properties at asymptotic radii are unobservable. With this point in mind, we computed observed projected properties at 0.25 and 4 effective radii,  $R_e$ , in order to look for the above mentioned correlations at observable limits for the five different sets of  $(a_1, a_2, a_3, a_4)$  which include one as in Fig. 1 and remaining four as in Fig. 2. To compute  $R_e$ , we fitted the azimuthally average surface density of our models to  $R^{1/4}$ -profile (de Vaucouleurs, 1948) between the interval  $0.25R_e \leq R \leq 4R_e$  and evaluated  $R_e/b_o$  that depends on the intrinsic axial ratios and viewing angles for each of five adopted sets of constant parameters  $(a_1, a_2, a_3, a_4)$ . In the spherical limit of our model,  $R_e/b_o$  is found to be  $\sim 4.4$ . However, it is also found that  $R_e/b_o$  of our triaxial models do not vary much from its value calculated in the spherical limit. Even then, we computed  $R_e/b_o$  for entire permitted range of intrinsic axial ratios and viewing angles for each set of  $(a_1, a_2, a_3, a_4)$  so that its exact value could be incorporated in calculations of correlations. Furthermore, we defined new parameter  $(b/a)_{diff} = (b/a)_{.25R_e} - (b/a)_{4R_e}$ , which exhibits ellipticity variation, and then found that the parameters  $(b/a)_{4R_e}$  and  $(b/a)_{diff}$  are the better choice to represent the desired correlations.

In Fig. 4, we have shown the correlations between  $(b/a)_{4R_e}$  and  $(b/a)_{diff}$  for different choice of intrinsic axial ratios  $p = p_o = p_\infty$  and  $q = q_o = q_\infty$  roughly covering the parameter space of  $1 \geq p \geq q \geq 0.5$  when our model with constant parameters  $(a_1, a_2, a_3, a_4)$  as in Fig. 1 is projected with varying viewing angles. We found that our model exhibits strong correlations which occupy well-separated regions in the parameters space of  $(b/a)_{4R_e}$  and  $(b/a)_{diff}$  for different choices of  $(p, q)$ .

It is interesting to note here that our model with remaining four values of  $(a_1, a_2, a_3, a_4)$  also show the qualitatively similar correlations as those found in Fig. 4. However, instead of considering all choices of  $(p, q)$  as in Fig. 4, we have presented them for only two choices of  $(p, q) = (0.65, 0.60)$  and  $(p, q) = (0.95, 0.60)$  in Figs. 5 and 6, respectively. The former choice of  $(p, q)$  represents highly prolate triaxial model, whereas the later choice of  $(p, q)$  corresponds to highly oblate triaxial one. Thus, these two choices of  $(p, q)$  are used to present non-overlapping correlations between a highly prolate and a highly oblate triaxial models that can be seen by comparing each plot of Fig. 5 with that of Fig. 6.

Besides above found correlations where  $\Delta p = |p_o - p_\infty| = 0$  and  $\Delta q = |q_o - q_\infty| = 0$  are taken, it has also been seen that the correlation patterns still maintain as long as  $\Delta p$  and  $\Delta q$  are considered as 0.05.

Finally, we have also examined the correlation plots by taking position angle

difference  $pa_{diff} = (\Theta_{*o} - \Theta_{*\infty})$  as one of the observable parameters. Correlation plots between position angle difference  $pa_{diff}$  and  $(b/a)_{diff}$  for a highly prolate triaxial and a highly oblate triaxial are presented in Fig. 7 where constant parameters  $(a_1, a_2, a_3, a_4)$  are same as in Fig. 1. Although some differences in the patterns between a highly prolate and a highly oblate triaxial are exhibited, they occupy overlapping regions. This suggests that  $pa_{diff}$  is not a suitable observed parameter to develop well-separated correlations for two different choices of  $(p, q)$  required for the shape determination.

But the non-overlapping correlations between the observed parameters  $(b/a)_{4R_e}$  and  $(b/a)_{diff}$  are appeared to be useful in the prediction of the intrinsic shapes of the mass models by mean of the graphical method of shape estimate of SF94.

Despite the radial profiles of projected properties of our models are much different from those of CT00, its correlations between  $(b/a)_{4R_e}$  and  $(b/a)_{diff}$  for different choices of  $(p, q)$  are found to be qualitatively similar to those shown in Fig. 1 of TC01 for CT00 model. This gives clear indication that our models can be good candidate for generating the ensembles of models, by considering different choices of  $\Delta p$  and  $\Delta q$  for each set of constant parameters  $(a_1, a_2, a_3, a_4)$ , which could be useful in the technique of TC01 in order to get the model independent shape estimate of a model galaxy. To get more insight over this issue, an experiment to recover the intrinsic shape of a model galaxy is presented in the next section where we have used Bayesian statistics and exploited the correlations by employing the above mentioned observed parameters and ensembles of models.

### 4.3 Recovery of the intrinsic shape of a model galaxy

In order to get an estimate of the intrinsic shape of a model galaxy, we followed Statler (1994a,b, hereafter, ST94a,b) who used Bayesian statistics and considered photometric and kinematical data for estimating intrinsic shape of an individual galaxy. Moreover, he considered models of the type  $\rho = \rho(m^2)$ , which give rise to concentric and coaligned ellipsoids, and used a constant value of ellipticity for a galaxy under consideration.

In our present study of the shape estimate of a model galaxy, we do not use any kinematical data. Rather, we have incorporated the variations in ellipticity by considering  $(b/a)_{4R_e}$  and  $(b/a)_{diff}$  as the observed parameters which are calculated from our present model by using following intrinsic parameters:  $p_\infty$ ,  $q_\infty$ ,  $\Delta p$ ,  $\Delta q$ ,  $(\theta', \phi')$  and  $(a_1, a_2, a_3, a_4)$ . Here  $p_\infty$  and  $q_\infty$  are regarded as the shape parameters, while except of  $(\theta', \phi')$ , the remaining intrinsic parameters are useful to generate ensembles of models.

We launched a test case and considered an oblate triaxial galaxy from our mod-

els with  $p_\infty = 0.95$ ,  $q_\infty = 0.60$ ,  $\Delta p = 0$ ,  $\Delta q = 0$ ,  $(\theta', \phi') = (35^\circ, 10^\circ)$  and constant parameters  $(a_1, a_2, a_3, a_4) = (0.2, 0.9, 0.2, 0.9)$ . The observed parameters of this selected model galaxy are found to be  $(b/a)_{4R_e} = 0.9398$  and  $(b/a)_{diff} = -0.0597$ . We allowed a typical error of 0.01 (e.g., de Carvalho et al., 1991) in ellipticities evaluated at  $0.25R_e$  and at  $4R_e$  which in turns set errors of 0.01 and 0.014 for  $(b/a)_{4R_e}$  and  $(b/a)_{diff}$ , respectively.

In order to estimate the shape of this galaxy, we considered our present models with five different sets of constant parameters  $(a_1, a_2, a_3, a_4)$  as adopted in the preceding sections. For each choice of  $(a_1, a_2, a_3, a_4)$ , we choose  $\Delta p \geq 0$  and  $\Delta q \geq 0$  in such a way that for each  $(p_\infty, q_\infty)$ ,  $(p_o, q_o)$  are taken as  $(\alpha p_\infty, \beta q_\infty)$  where choices of  $(\alpha, \beta)$  are  $(1, 1)$ ,  $(1.05, 1)$ ,  $(0.95, 1)$ ,  $(1, 1.05)$ ,  $(1, 0.95)$ . This gives the ensembles of models for a chosen value of  $(p_\infty, q_\infty)$ . For each model with a particular value of  $(p_\infty, q_\infty)$  and above given observed parameters and errors, we estimated the likelihood  $L$  of obtaining the observed data from the model and the posterior density  $P$ , which is the product of likelihood  $L$  and the prior density  $F$ , by the formulas given in ST94a,b. We assumed maximum ignorance of  $F = (\sin \theta' / 4\pi) F_s$  by considering  $F_s = \text{constant}$  (cf. ST94b). We then integrated the posterior density  $P$  over the viewing angles  $(\theta', \phi')$  and added it for different choices of  $(\alpha, \beta)$  and constant parameters  $(a_1, a_2, a_3, a_4)$ . We plotted the resultant posterior density as a function of  $(p_\infty, q_\infty)$  which is shown by dark-grey shade in Fig. 8. Here the darker shade corresponds to the higher posterior density. The inner and outer constant  $P$  contours, enclosing 68% and 95% of the resultant posterior density, show  $1\sigma$  and  $2\sigma$  error-bar regions, respectively. It is clear that the true shape of a model galaxy, indicated by a white cross, lies within the  $1\sigma$  region. We also found that the resultant posterior density is sharply peaked function of the shape parameters  $(p_\infty, q_\infty)$  since the  $1\sigma$  region is sufficiently narrow. This satisfies the necessary condition of Bayesian statistics that the resultant posterior density to be relatively insensitive to the prior density in order to get the ‘likelihood dominated’ posterior density.

## 5 Summary and discussion

We have constructed a family of triaxial models by inclusions of additional radial functions, each multiplied by a low-order spherical harmonic, in the models of CT00. This procedure of building triaxial models by addition of the additional radial functions was initially suggested by TC01 to enlarge the ensembles of models in their technique of intrinsic shapes determination of model galaxies. Projected surface density  $\Sigma$  of our present triaxial models can be calculated analytically which allow us to derive the analytical expressions of  $b/a$  and  $\Theta_*$  at asymptotic radii. However, the approximate elliptical isodensity contours of  $\Sigma$  show the variations in  $b/a$  and  $\Theta_*$  as functions of  $R$ . This

suggests that our triaxial models can be considered as simple analytical models exhibiting ellipticity variations and isophotal twists. We have also studied the effects of the additional radial functions on the profiles of  $b/a$  and  $\Theta_*$  by considering different choices of constant parameters  $(a_1, a_2, a_3, a_4)$ . In this regard, different trends of the profiles of  $b/a$  and  $\Theta_*$  are found for different contributions of additional radial functions. Furthermore, the profiles of  $b/a$  and  $\Theta_*$  show small scale variations at inner  $R$  which are also seen in many real elliptical galaxies. Thus, our models can be useful to compare with observed photometric properties of real elliptical galaxies.

TC01 pointed out that more ensembles of models, showing correlations between the observed parameters for different choice of intrinsic parameters, are necessary to be explored to make their method of shape estimation more reliable. In this regard, our models seem to be good candidate for providing another set of ensembles of models in the method of TC01, since result of shape estimation of a model galaxy using ensembles of our models is found to be satisfactory by utilizing the strong correlations between  $(b/a)_{4R_e}$  and  $(b/a)_{diff}$ . But it would be wise to look for larger sets of ensembles of models representing correlations between observed properties that could be useful in satisfactory determination of the shape of model galaxies before going ahead to apply this method of shape estimation to real ellipticals.

## Acknowledgements

MD expresses her sincere thanks to PNU (Pusan National University, Busan, Korea) for providing financial support through the postdoctoral fellowship. PT would like to express his sincere thanks to ARCSEC (Astrophysical Research Center for the Structure and Evolution of the Cosmos, Seoul, Korea) for providing financial support through the postdoctoral fellowship which made this study possible. HBA thanks the Korea Science Engineering Foundation (KOSEF) for the support provided through grant No. R01-1999-00023.

## References

- Chakraborty, D.K., & Thakur, P. 2000, MNRAS, 318, 1273 (CT00)
- De Carvalho, R.R., Djorgovski, S., da Costa, L.N., 1991, ApJS, 76, 1067
- De Vaucouleurs, G., 1948, Ann. Astrophys., 11, 247
- De Zeeuw, P.T., Carollo, C.M., 1996, MNRAS, 281, 1333 (ZC96)
- De Zeeuw, P.T., Franx, M., 1989, ApJ, 343, 617
- De Zeeuw, T., Merritt, D., 1983, ApJ, 267, 571
- Schwarzschild, M., 1979, ApJ, 232, 236

Statler, T.S., 1994a, ApJ, 425, 500 (ST94a)  
Statler, T.S., 1994b, AJ, 108, 111 (ST94b)  
Statler, T.S., Fry, A.M., 1994, ApJ, 425, 481 (SF94)  
Thakur, P., & Chakraborty, D.K. 2001, MNRAS, 328, 330 (TC01)

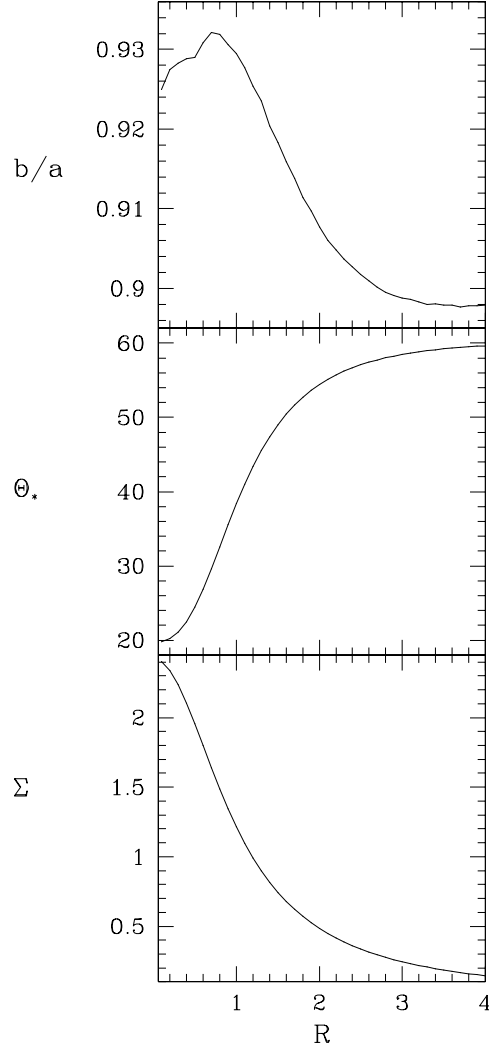


Fig. 1. Profiles of  $b/a$ ,  $\Theta_*$  and  $\Sigma$  as functions of  $R$  for a model with the intrinsic parameters  $(p, q, \theta', \phi') = (0.65, 0.60, 60^\circ, 10^\circ)$  and the constant parameters  $(a_1, a_2, a_3, a_4) = (0.2, 0.9, 0.2, 0.9)$ . Here  $\Theta_*$  is in degree, whereas  $R$  and  $\Sigma$  are in the units  $b_o$  and  $M/4\pi b_o^2$ , respectively. Like  $R$ , the constant parameters  $(a_1, a_2, a_3, a_4)$  are also given in the units of  $b_o$ .

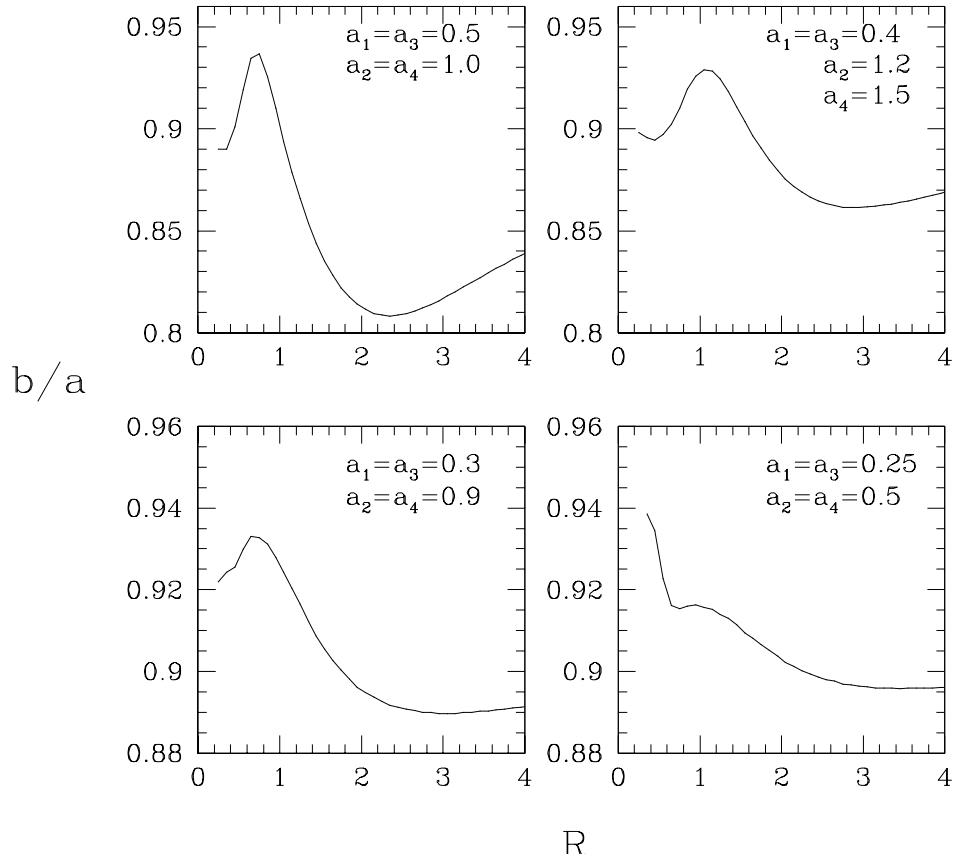


Fig. 2. Profiles of  $b/a$  as functions of  $R$  for four different choices of the constant parameters  $(a_1, a_2, a_3, a_4)$ . The adopted values of  $(a_1, a_2, a_3, a_4)$  are given in top right corner of each panel, whereas the remaining intrinsic parameters of model, i.e.,  $(p, q, \theta', \phi')$ , are same as those in Fig 1. Here  $R$  and constant parameters  $(a_1, a_2, a_3, a_4)$  are given in the units of  $b_o$ .

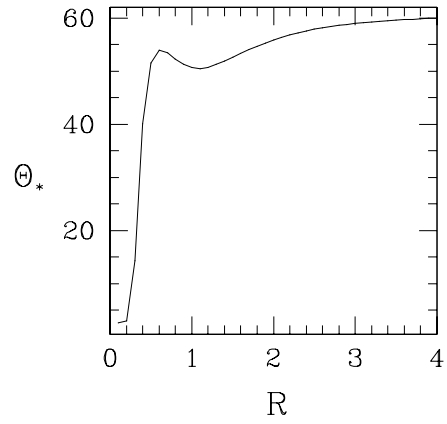


Fig. 3. Profile of position angle  $\Theta_*$  as a function of  $R$ . The intrinsic and constant parameters of model are same as those adopted in the bottom right panel of Fig 2. Units of  $R$ ,  $\Theta_*$  and constant parameters ( $a_1, a_2, a_3, a_4$ ) are same as those given in Fig. 1.

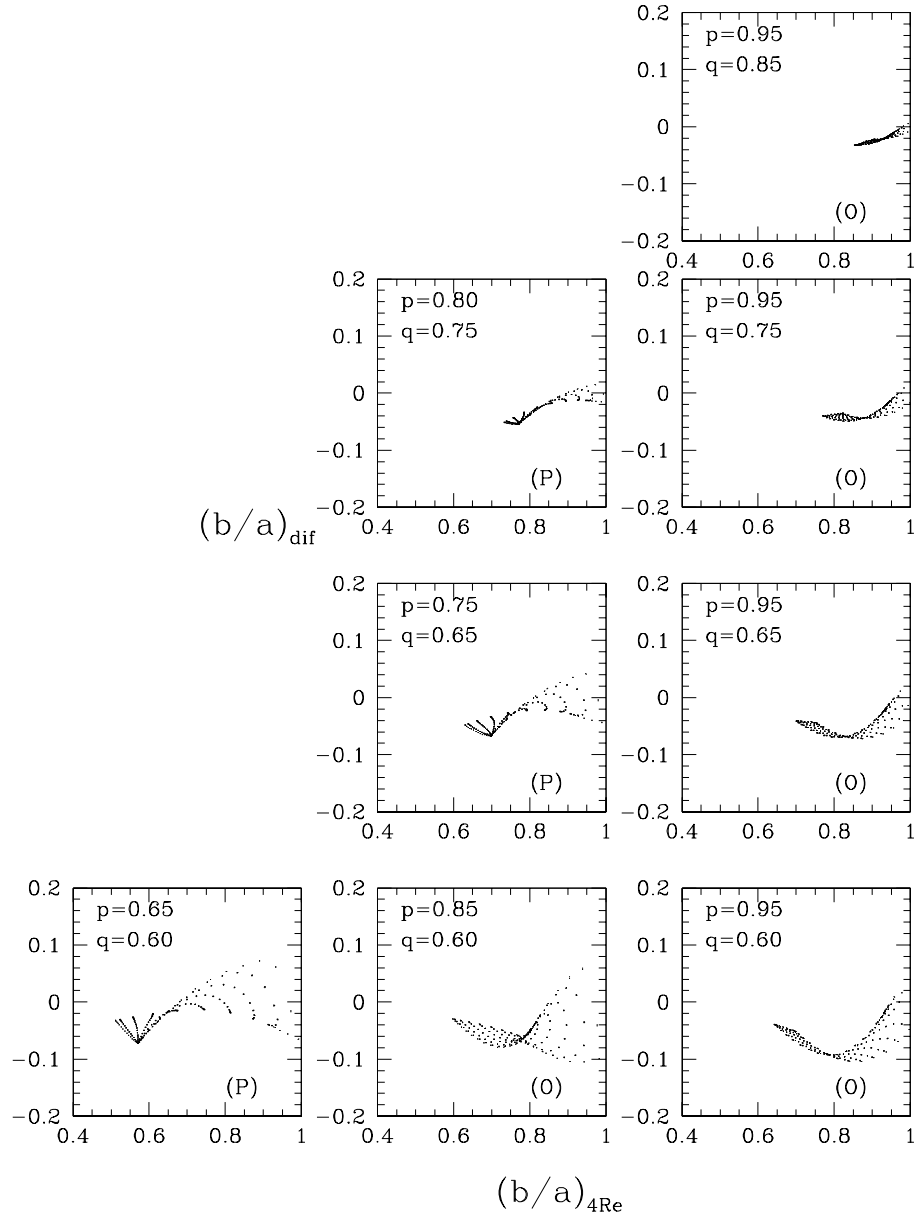


Fig. 4. Each panel shows correlation between  $(b/a)_{4Re}$  and  $(b/a)_{diff}$ , when a model with a particular value of  $(p, q)$  is projected at various viewing angles. Considered values of  $(p, q)$  are indicated in top left corner of each panel, whereas constant parameters  $(a_1, a_2, a_3, a_4)$  are same as those adopted in Fig. 1.

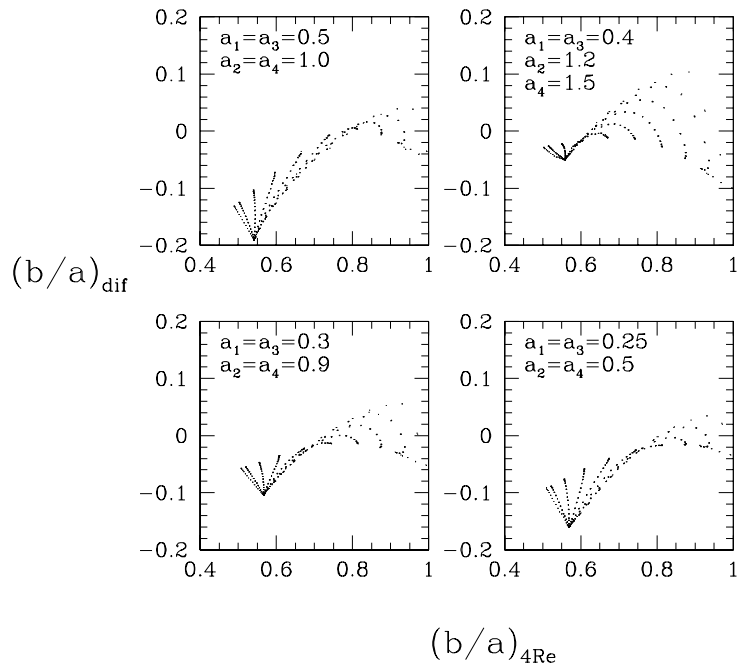


Fig. 5. Correlation between  $(b/a)_{4Re}$  and  $(b/a)_{dif}$  for the fixed values of  $(p, q) = (0.65, 0.60)$  but for different choices of constant parameters  $(a_1, a_2, a_3, a_4)$  as indicated in top left corner of each panel.

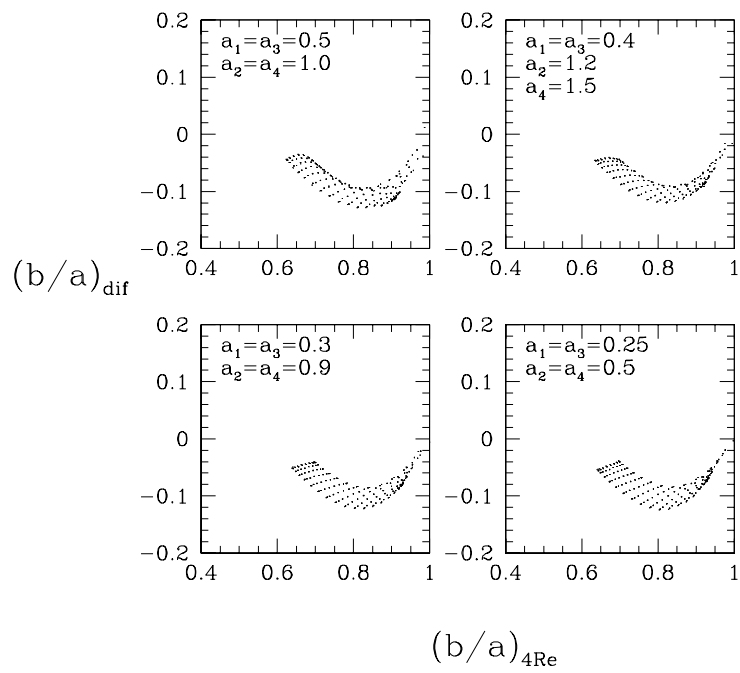


Fig. 6. Correlation plots as in Fig. 5 but for  $(p, q) = (0.95, 0.60)$ .

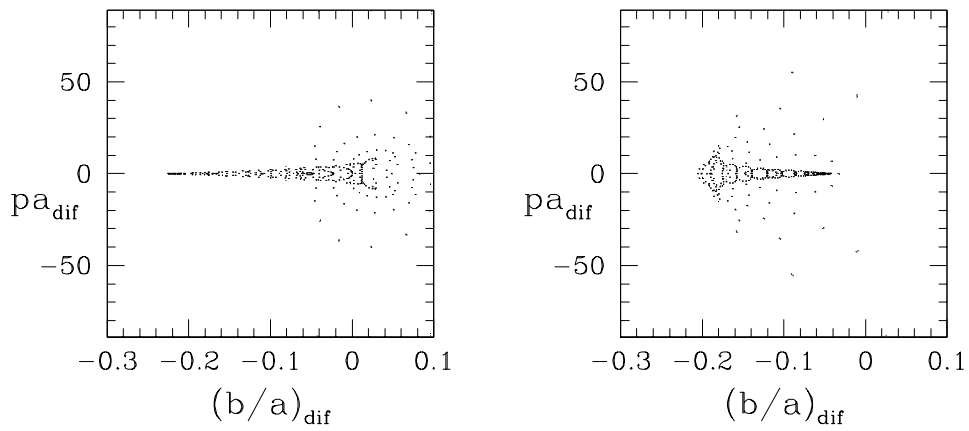


Fig. 7. Correlation plots between  $(b/a)_{dif}$  and  $pa_{dif}$ . The left panel represents correlation for model with  $(p, q) = (0.65, 0.60)$ , whereas the right panel shows it for  $(p, q) = (0.95, 0.60)$ . Constant parameters  $(a_1, a_2, a_3, a_4)$  are same as those adopted in Fig. 1.

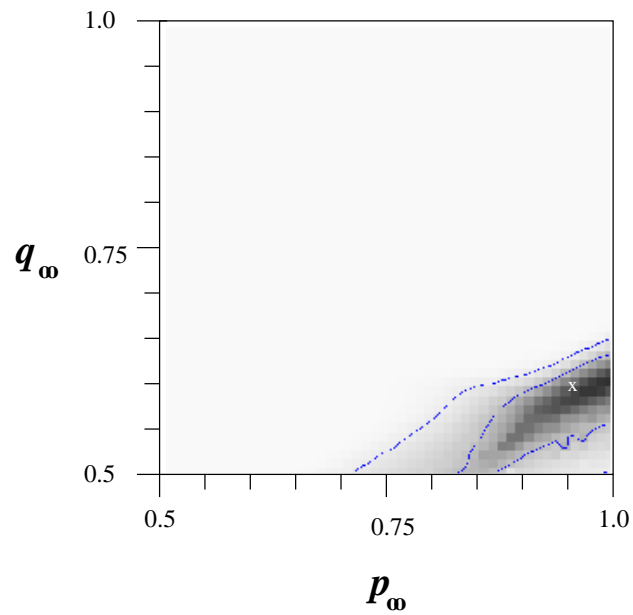


Fig. 8. Shape estimate of a model galaxy using ensembles of models. A white cross represents the true shape of a model galaxy. Inner and outer contours represent  $1\sigma$  and  $2\sigma$  error-bar regions, respectively.